Available online at www.sciencedirect.com

ScienceDirect

Procedia Engineering 213 (2018) 630–643

Procedia Engineering

www.elsevier.com/locate/procedia

7th International Conference on Fatigue Design, Fatigue Design 2017, 29-30 November 2017, Senlis, France

# Effect of porosity on the fatigue strength of cast aluminium alloys: from the specimen to the structure

Pierre OSMOND[a,*], Viet-Duc LE[a,b,c], Franck MOREL[b], Daniel BELLETT[b] and Nicolas SAINTIER[c]

[a]*PSA Groupe, 18 rue des fauvelles, 92256 La Garenne-Colombes cedex, France*
[b]*Arts et Métiers ParisTech, Campus Angers – Laboratoire LAMPA – 2 Bd du Ronceray, 49035 Angers Cedex 1, France*
[c]*Arts et Métiers ParisTech, Campus Bordeaux – Laboratoire I2M – Esplanade des Arts et Métiers, 33405 TALENCE Cedex, France*

**Abstract**

The fatigue strength of cast aluminium alloys is known to be greatly affected by different defect types related to the manufacturing process, particularly microshrinkage pores created during the solidification phase of the casting process. Even if certain classification procedures are given in the standard ASTM E155-15 [1], the presence of defects is not readily related to the capacity of a component or a structure to meet the requirements of the mechanical technical specifications.

The present study aims at establishing a clear link between certain microstructural features and the average fatigue strength. This is possible by looking for the average size of critical defects and using a relevant statistical analysis. More exactly, the Murakami approach based on the statistics of extremes is employed. The main originality of this work lies in the application of this approach to the case of a real structure submitted to high cycle fatigue damage: engine cylinder heads, used in the automotive industry. Indeed, both fatigue tests and microstructural characterizations are carried out on cylindrical specimens and real structures. The specimens are subjected to uniaxial and multiaxial loading conditions [2]. Original fatigue tests, developed by PSA to load in-service critical regions, are carried out on cylinder heads. Systematic analyses of fatigue failure surface are conducted to obtain the statistics of critical defects at the origin of the failures for both specimens and structures.

In parallel, critical regions and the associated local loading mode in the structure are characterized by an appropriate high cycle fatigue analysis. The latter, combined with the fatigue test data and the statistical analysis of the critical defects, leads to a discussion about the size effect and an approach is proposed for a relevant fatigue design procedure.

© 2018 The Authors. Published by Elsevier Ltd.
Peer-review under responsibility of the scientific committee of the 7th International Conference on Fatigue Design.

*Keywords:* High cycle fatigue, Cast aluminium alloys, Defect containing materials, Size effect, Fatigue design procedure

1877-7058 © 2018 The Authors. Published by Elsevier Ltd.
Peer-review under responsibility of the scientific committee of the 7th International Conference on Fatigue Design.
10.1016/j.proeng.2018.02.059

## 1. Introduction

The cast aluminium alloys are widely used in automotive industry due to their relative good strength combined with a low density and an excellent conductivity. These alloys are commonly employed for chassis and engine components which are, for the most part, subjected to mechanical cyclic loads and present a serious risk of mechanical fatigue. In order to avoid fatigue crack initiation and ensure the component resistance, appropriate design methodologies have to be developed. They are mostly based on an appropriate fatigue criterion, whose identification is carried out by fatigue tests performed on test specimens, who's size is generally quite different to the size of the fatigue critical zones found on the real manufactured components.

The fatigue strength of cast aluminium alloys is known to be greatly affected by different types of microstructural heterogeneities due to the manufacturing process. According to this process and subsequent treatment, the microstructural features can be significantly modified especially in terms of eutectic components (silicon particles and iron-based intermetallics) and casting defects, notably micro-shrinkage pores and gas porosity. Despite the significant effort to characterize and understand the influence of these microstructural heterogeneities on the High Cycle Fatigue (HCF) behaviour of these alloys [2][7], the development of design methodologies taking into account the effect of defects on the fatigue life prediction of structures is still under progress [8][10]. However, in spite of the presence of defects, car manufacturers must ensure a targeted level of reliability of their components and structures. In the case of pores, manufacturers set up control procedures via X-ray inspection for defect detection and to reject components containing defects presenting an unacceptable risk of failure. Even if some classification procedures are given in the standard ASTM E155-15 [1], the presence of defects cannot be readily related to the capacity of a component or a structure to meet the requirements of the mechanical technical specifications. Thus, the definition of material defect requirements is in most cases based on the manufacturers experience, without quantitative justification. With a yearly production of 3 million engines, the optimization of production costs is a major challenge for the PSA Groupe. This justifies the need to development methods to define robust acceptance criteria.

A first step is to provide a clear link between defect features and the fatigue strength. This requires a precise understanding of the fatigue damage mechanisms associated with the microstructural features under high cycle fatigue loading conditions. This has been done for three different aluminium alloys in previous work undertaken by the authors [2][11].

The present study aims at establishing a link between features of the micro-shrinkage porosity and the average fatigue strength. This is done by using the classical approach introduced by Murakami [12] and formalized in the international ASTM standard [13]. It is applied to both test specimens and a real structure: an engine cylinder head. The use of a real structure is the opportunity to highlight the possible size effect between the test specimens used to identify the fatigue criterion and the component to be designed. The capacity of the method to account for different defects distribution parameters is tested by applying the approach to two aluminium alloys elaborated by different casting processes: gravity die casting and gravity lost foam casting. Throughout this exercise, the method proposed by Murakami to extrapolate the average size of the critical defects to objects to other dimensions is compared to the alternative method proposed by Makkonen [14]. Finally, based on the joint analyses of the average critical defect size in the specimens and the structure, a relevant fatigue design procedure accounting for size effect is proposed.

## 2. Materials & experimental conditions

### *2.1. Materials microstructure and properties*

Two cast aluminium alloys, referred to as alloys A and B, are investigated in this study. These denominations are consistent with those used in the other published results [2][9][15]. These alloys were elaborated by either gravity die casting or lost foam casting and were both subjected to a T7 treatment.

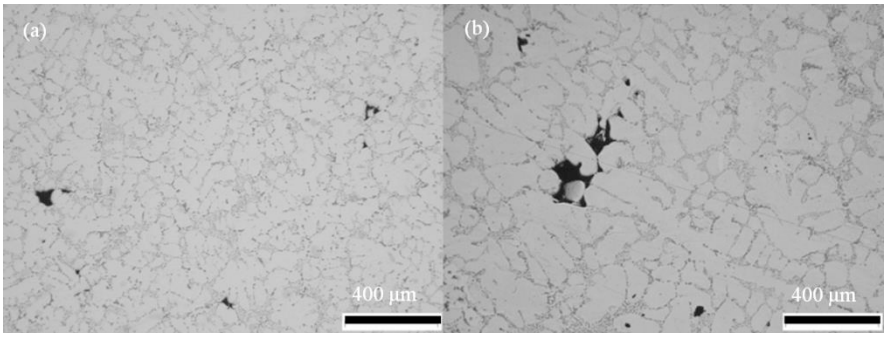


Figure 1 : Typical microstructure of two studied alloys. (a) AlSi7Cu0.5Mg0.3 KT7 DC, (b) AlSi7Mg0.3 ST7 LFC

The characteristics of each casting process, including notably an important difference in solidification time, lead to two materials with significantly different microstructures. Typical microstructures of these two alloys are presented in Figure 1. As an initial approach these differences can characterised in terms of the Secondary Dendrite Arm Spacing (SDAS). This quantity is determined by identifying individual aluminium dendrites; the linear intercept method is then used to measure the SDAS. Forty dendrites of each material were analysed to assess the average SDAS.

The chemical composition, casting process, heat-treatment and SDAS of each material are summarized in the Table 1.

| Alloy | Main elements of the composition (%W) | Casting Process | Heat treatment | SDAS (µm) |
|---|---|---|---|---|
| A | 7%Si, 0.5%Cu, 0.3%Mg, Sr-modified | Gravity Die Casting | T7 | 42.3±9.7 |
| B | 7%Si, 0.3%Mg, Sr-modified | Lost Foam Casting | T7 | 77.3±18.9 |

Table 1 : Materials, chemical composition, casting process, heat treatment and SDAS.

Alloy A is fully representative of what can be found in industrial components. Indeed, all the specimens used for both microstructural analysis and fatigue tests were extracted from cylinder heads. In order to have a much larger volume from which fatigue specimens could be extracted, the industrial casting process was slightly modified with negligible microstructural changes to the alloy. The test specimens were then extracted from the component in close proximity to critical areas for fatigue failure.

Faced with the difficulty of modifying the mould used to produce lost foam casted cylinder heads, a mould in the form of a plate was preferred. Consequently, and due to the substantial difference in geometry and volume between the cylinder heads and the used mould, it should be noted that the microstructure and defect population of alloy B are not representative of the material present in manufactured components.

### *2.2. Pore populations and critical defects characterization*

Pore populations and critical defects were characterized using two different methods. The analysis of the pore distribution is based on the metallography methodology proposed by Murakami [12]. This analysis is conducted through optical microscopic observations of polished samples. On each sample, several observations are performed, using a constant inspection area $S_0$. Only the largest pore of each optical micrograph is considered for the morphological analysis (Figure 2.a), in order to derive the extreme value distribution of the pore size.

The critical defect characterization is based on the analysis of fatigue failure surfaces of specimens tested in fatigue. Each specimen is examined to identify and measure the size of the casting defect at the origin of the fatigue failure for alloys A and B (Figure 2.b). When several cracks can be found on the fatigue failure surface, only the

defect at the origin of the principal crack is considered. In cases where several defects can be found for the same crack, defects located near the surface are considered. The main reason for this is that cracks preferentially initiate at surface or sub-surface defects [15][19].

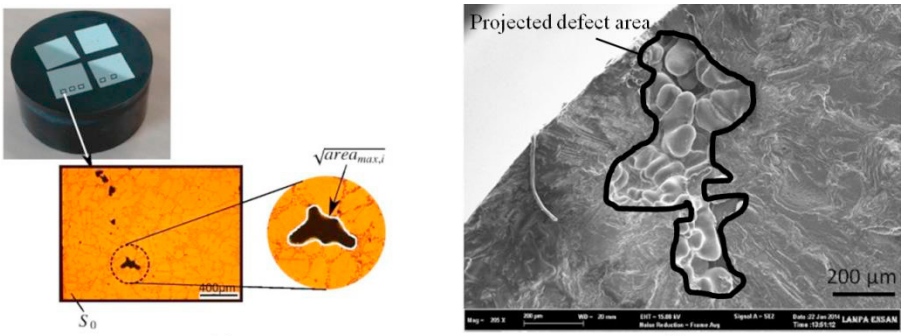


Figure 2 : Illustration of casting defects characterization methodologies. (a) The Murakami methodology, (b) Critical defect on a fatigue failure surface.

### *2.3. Experimental conditions*

#### *2.3.1. Fatigue tests on specimens*

All the fatigue tests shown below were performed at ambient temperature on a Rumul resonant testing machine at 90-110 Hz. All fatigue tests were conducted with the same specimen geometry, available in [2], in order to eliminate any size effect. Two loading conditions, combined tension-torsion with a biaxiality ratio of 0.5 and uniaxial loading, are investigated in this contribution. For each loading condition, between 15 and 20 specimens have been tested. All the fatigue tests were conducted under symmetrical alternate load (*R=-1*), using a staircase technique, to assess the fatigue strength at $2.10^6$ cycles. A step of 10 MPa was used for the staircase protocol. The stopping criterion was chosen to ensure the presence of a fatigue crack of approximately 3 mm in length.

In order to characterize the influence of defects of the fatigue strength, all the specimens that survived in the staircase procedure were retested at a stress amplitude one step higher for an additional $2x10^6$ cycles. This was repeated until failure was observed and the stress level of the final step was taken as the fatigue strength [16]. This method is regularly used to investigate the effect of defects on the fatigue strength.

#### *2.3.2. Fatigue tests on cylinder head*

Fatigue tests were performed at ambient temperature on a cylinder head made of alloy A. These tests are carried out for each new engine development in order to assess the mean fatigue strength of the component. This test simulates, in a simplified manner, the effective loading present during in-service loading conditions, especially the pressure loading due to combustion. Even if the test conditions are quite far from in-service conditions, this test enables loading the critical zones as closely as possible to the in-service conditions, particularly in terms of the size of the loaded zones and the stress gradients. The integration of such tests in the cylinder head validation protocol is of particular importance as they provide an efficient tool for the validation of the numerical design methodology and to prevent major design errors.

Four metallic blocks positioned on the contact surfaces of the cylinder mounting screws (highlighted in green in Figure 3-b) are used as supports. The load is applied by a vertical force on the center of the fire deck for each cylinder using a die centered on the spark plug hole (see Figure 3-a). Though simple, these boundary conditions result in realistic stress states in the critical zones, located on water side of a cooling passage (see Figure 3.c).

All the fatigue tests were conducted with a positive load ratio (*R=0.1*), using the staircase technique, to assess the fatigue strength at $2x10^6$ cycles. As the presence of a fatigue crack cannot be detected during the test, all the tests are

conducted up to $2x10^6$ cycles. The presence of a fatigue crack is analyzed after the test, by cutting of cylinder heads then by dye penetrant liquid examination and, if necessary, opening of cracks.

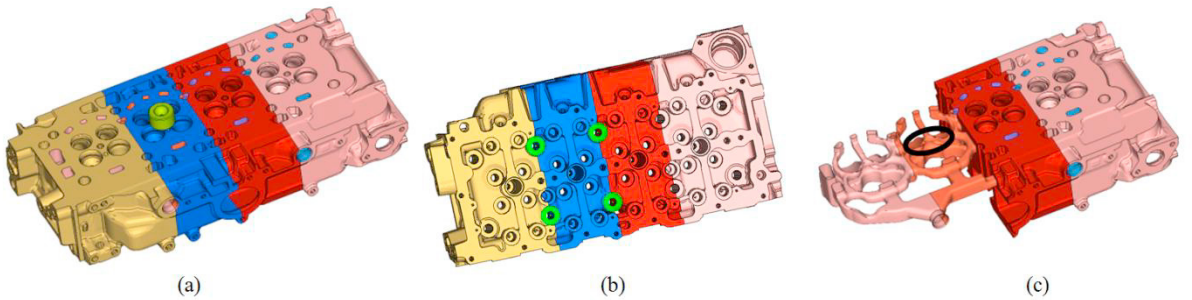


Figure 3 : Illustration of cylinder head testing conditions. Location of (a) application of the force, (b) supports and (c) approximate location of the critical zones.

## 3. Assessment of average critical defect size

### *3.1. High cycle fatigue damage mechanisms and key microstructural defects feature*

The HCF behaviour and associated damage mechanisms under various uniaxial and multiaxial loading modes, for different mean stress levels, for the two investigated alloys have been analysed in previous studies [2][3][11][17][18]. These studies have highlighted the important influence of microstructural heterogeneities on the HCF strength and have shown the coexistence of two damage mechanisms depending on the loading modes:

- For loading conditions with significant level of hydrostatic stress cracks initiate at micro-shrinkage pores and propagate due to a crack opening mode.
- For pure torsional loads, cracks may also initiate at persistent slip band resulting from local plastic activity and propagate initially in a shear mode.

This analysis of the influence of micro-shrinkage pores on the fatigue strength is based on a precise analysis of the micro-shrinkage pore populations. According to the procedures used (2D or 3D), various morphological features are available such as the volume, area, equivalent radius, Feret diameter, sphericity, etc.. Among all these morphological features, the square root of the initial defect projected area is known to be a relevant controlling parameter for the high cycle fatigue strength [12] and is used by the authors to characterize the influence of natural defects on fatigue strength. In the remainder of this communication, the defect size is presented in terms of the square root of the initial defect projected area.

The pore size distribution determined by the metallography method proposed by Murakami is shown in fig. 4 for both alloys A and B. These distributions are compared to those obtained by observations of critical defects on the failure surfaces of tested specimens. Between 70 and 110 defects have been analysed for the metallography methodology, the critical defect distributions are identified from the analysis of 35 to 40 fatigue failure surfaces.

It is shown that the defect sizes measured by the second method are much larger than those obtained by the first method. This is a clear example of a size effect. Indeed, the distribution obtained by the first method corresponds to the extreme value distribution related to the inspection area $S_0$ while the distribution determined by the second method is related to the critical loaded volume of the tested specimen. Because the sizes of these two observation zones are very different, the maximum defect sizes observed are different.

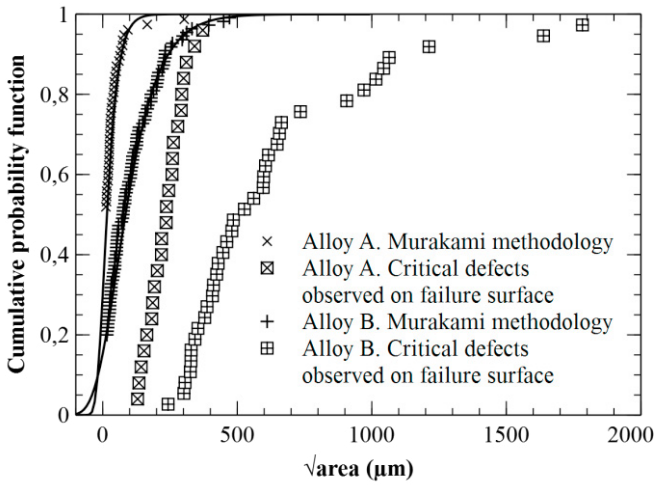


Figure 4 : The defect size distribution for alloys A and B characterized by the Murakami methodology and an analysis of the fatigue failure surfaces.

Because these distributions correspond to extreme value distributions, the Gumbel distribution has been used to fit the experimental data. The Gumbel distribution is expressed as:

$$F\left(\sqrt{area}_{\max}\right) = \exp\left\{-\exp\left(\frac{-\left(\sqrt{area}_{\max} - \mu\right)}{\beta}\right)\right\} \qquad (1)$$

Where $\mu$ and $\beta$, are the location and the scale parameters, respectively. These parameters are identified using the distributions characterized by the Murakami methodology. The values for alloys A and B are given in Table 2.

| Alloy | $\mu$ | $\beta$ |
|---|---|---|
| A | 4.17 | 27.78 |
| B | 52.10 | 84.03 |

Table 2 : Values of $\mu$ and $\beta$ *identified on alloy A and B using the pore size distributions* obtained by 2D metallography methodology.

As shown on Figure 4, good agreement is observed between the Gumbel distribution and the experimental data.

### *3.2. Methodologies for the prediction of the maximum pore size in a given volume*

The comparison of the pore size distributions characterized by the Murakami methodology and an analysis of the fatigue failure surfaces highlights an important size effect. To address this issue, two methods are tested to extrapolate the fatigue critical defect size from the 2D metallography analyses:

- the normalised method, originally introduced by Murakami [12] and formalized in the international ASTM standard [13]
- the alternative method proposed by Makkonen and al [14].

These two methods are based on the theory of extremes and assume that the defect size distribution is independent of the size of the considered object.

The normalised method is based on the concept of a return period T defined as [12][13] :

$$T = \frac{S}{S_0} \tag{2}$$

Where S is the area of interest and $S_0$ is the inspection area. Assuming that the distribution function for the presence of the largest defect $\sqrt{area_{\max}}$ on a surface of size S can be expressed as [12]:

$$F\left(\sqrt{area_{\max}}\right) = \frac{T-1}{T} \tag{3}$$

the largest characteristic defect size associated with a surface S can be calculated as:

$$\sqrt{area_{\max}} = \mu + y_T \beta \tag{4}$$

With $y_T$ is the reduced variable and is expressed as:

$$y_T = -\ln\left(-\ln\left[\frac{T-1}{T}\right]\right) \tag{5}$$

Where $\mu$ and $\beta$ are the Gumbel distribution parameters identified on the pore size distribution characterized by the Murakami methodology.

As the description of a defect is a volumetric problem, Murakami proposes an extension of this methodology to deal with the 3D-problem. To achieve this, the authors assume that the inspection volume $V_0$ is equal to the product of the inspection area $S_0$ multiplied by the average largest pore size identified on the inspection area $S_0$. The return period T can then be expressed as:

$$T = \frac{V}{V_0} \tag{6}$$

This methodology has been recently discussed by Makkonen et al [14]. They outlined several problems regarding the normalised approach. Among these are the fact that an extrapolation from a large area/volume to a smaller area/volume is not possible and the fact that it is impossible to link the largest defect extrapolation to a specific probability of occurrence.

To address these issues, an alternative approach has been proposed by the authors. Based on the weakest link concept, the distribution function of largest defect size distribution in a volume $V$ is expressed as:

$$F\left(\sqrt{area_{\max}}, V\right) = F\left(\sqrt{area_{\max}}, V\right)^{V/V_0} \tag{7}$$

No longer limited to a single descriptive parameter, the largest defect size can then be described by an appropriate distribution, characterized by its mean, mode and median. For the case of Gumbel distribution used in the ASTM standard, the largest defect size distribution relative to the volume $V$ can be expressed as:

$$F\left(\sqrt{area_{\max}}, V\right) = \exp\left\{-\frac{V}{V_0}\exp\left(\frac{-\left(\sqrt{area_{\max}} - \mu\right)}{\beta}\right)\right\} \tag{8}$$

The average largest defect size can be obtained considering, for the Gumbel distribution, the quantile value of 0.57 :

$$\sqrt{area_{\max}} = -\beta \ln\left(-\frac{V_0}{V}\ln(0.57)\right) + \mu \qquad (9)$$

With $\mu$ and $\beta$ the Gumbel distribution parameters identified on the pore size distribution obtained by 2D metallography methodology.

### *3.3. Application to specimens*

These two approaches are used to assess the average critical defect size observed on the failure surfaces of the specimens tested in fatigue. The largest defect size distribution related to the analysis conducted by the metallography methodology is used as the basis of the extrapolation. The reference inspection volume is directly obtained from the inspection area $S_0$ and the associated average extreme defect size.

The definition of the targeted volume is discussed relative to the damage mechanisms. A simpler solution would be to choose the loaded volume of the specimens gauge section. Nevertheless, this choice is not supported by the damage mechanisms observed on the specimens. Indeed, the principal crack initiation occurs systematically on surface of sub-surface micro-shrinkage pores. For all of the tested specimens, no evidence of crack initiation and propagation from internal pores was found. This observation is consistent with observations reported in the literature [19]. In addition, for the materials studied here, an investigation by X-ray microtomography has been performed [15] and highlighted that, for the 7 scanned specimens, all the pores initiating fatigue cracks are located near the specimen surface with a maximum distance to the surface of approximatively 500 µm. Therefore, and as a first approach, the extrapolation of the critical defect size in tested specimens is conducted considering a subsurface volume with a thickness of 0.5 mm. It is important to note that this definition is associated with the analysed loading conditions, and does not take into account the presence of a stress gradient. A study is currently underway to better understand the influence of the gradient effect on the damage mechanisms and the fatigue strength.

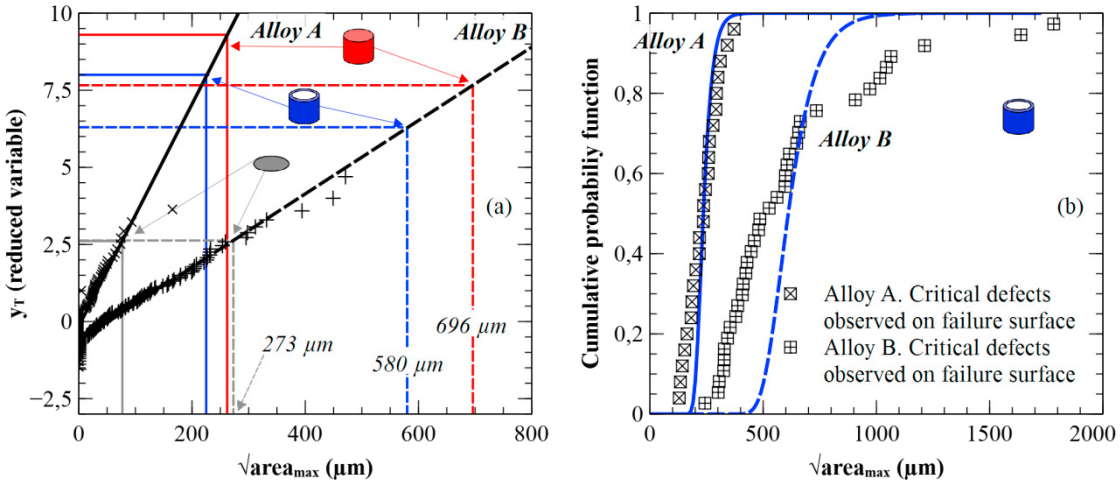


Figure 5 : (a) The normalised procedure, (b) The Makkonen approach. (a) The extreme defect average size as a function of the reduced variable $y_T$, for alloys A and B. Highlighting of the three cases studies (b) Comparison between the experimental and the extrapolated critical defect size distributions for alloys A and B. The extrapolations are based on the pore size distributions obtained by 2D metallography analysis considering a subsurface volume with a thickness of 0.5 mm.

Figure 5-a describes for alloys A and B, the effect of the sample size on the predicted average extreme defect size obtained using the normalised method. The three cases studies are presented in grey, red and blue respectively: grey corresponds to a disc with a diameter equal to that of the test specimen and a thickness *h*. Red corresponds to the total volume of the specimens reduced gauge section. Blue corresponds to a cylindrical subsurface volume with a thickness of 0.5 mm and a height equal to the specimen gauge length. Alloy A is depicted by solid lines and Alloy B by dashed lines. For both alloys, the effect of the sample size on the predicted average extreme defect size is

important. For the three cases studies, the difference between the estimated average extreme defect size can be up to a factor of 3. In terms of the absolute size, the effect is particularly significant for the alloy B, where the average extreme defect size changes from 273 µm for the disk, to 696 µm for the total volume of the reduced gauge section.

The Figure 5-b describes for alloys A and B, the results for the Makkonen approach. For each alloy, the extrapolation of the critical defects size distribution observed on failure surface of test specimens is compared with experimental data. The experimental distributions, already presented in Figure 4, are depicted by points, the predictions by lines. Even if good correlation is obtained for the median and average sizes, poor quality predictions are obtained for the complete distributions. This point deserves further investigation.

Table 3 summarizes the experimental and estimated average critical defect sizes, obtained using the normalised procedure and the Makkonen approach for alloys A and B. Good correlation is obtained between the experimental and the estimated average critical defect sizes, whatever the methodology used to account for the size effect. This good correlation seems to confirm the assumption of a sub-surface critical volume.

| Alloy | Average critical defect size ($\sqrt{\overline{area}_{max}}$) : Extrapolation from 2D measurements (µm) | | Average critical defect size ($\sqrt{\overline{area}_{max}}$) : Observations on failure surface (µm) |
|---|---|---|---|
| | Normalised procedure [13] | Makkonen et al. [14] | |
| A | 228 | 244 | 233 |
| B | 580 | 628 | 630 |

Table 3 : Comparison between the experimental and the estimated average critical defect sizes on specimens, obtained with standard procedure and Makkonen approach.

### *3.4. Application to a real structure: the cylinder heads*

- Damage mechanisms in the structure and experimental measurement of the average critical defect size

A similar analysis was carried out on cylinder heads tested in fatigue. Fatigue tests on 20 cylinder heads were completed and followed by the systematic observation of the failure surfaces in order to firstly identify fatigue crack initiation sites. The failure surface observations show that, for these tests which are representative of in-service loads, cracks always initiate from micro-shrinkage pores. These observations are in full agreement with observations on specimens. This confirms that the same initiation mechanism, initiation from micro-shrinkage pores, occurs in both the structure and specimens, for the loading conditions investigated here. Typical failure surface and crack initiation site observed on failure surfaces in the cylinder heads are given in **Erreur ! Source du renvoi introuvable.**-c and 6-d.

Based on this initial analysis, pores at the origin of the principal crack were measured to assess the average critical defect size in the cylinder heads. Note that the failure surfaces are not available for all tested cylinder heads because cylinder heads are destroyed to verify the presence of a crack. In addition, cylinder heads containing "small" fatigue crack of a length of less than 5 mm are preferred in order to facilitate the identification of the pores at the origin of the principal crack. Thus, in total 12 failure surfaces for 8 cylinders heads were analyzed to measure the average critical defect size. For several of these cylinder heads, two principal cracks can be observed, each located on a branch of the water core that surrounds the spark plug hole. These locations are in good agreement with critical areas predicted by the numerical simulation, as shown by figure 6-a. Finally, an experimental average critical defect size of *162 µm* is found, with values ranging from 110 to 280 µm. Note that this value is significantly smaller than the average critical defect size observed on the specimen failure surfaces.

- Numerical assessment of critical loaded volume

The critical loaded volume in the structure is assessed from finite element simulations. These simulations are performed on a complete cylinder head meshed with tetrahedral elements. The finite element mesh size is approximately 1 mm in the critical zone and 5 mm in the coarsest areas. “C3D10” elements and “M3D6” membrane elements are used to determine the mechanical response of the bulk material and the surface respectively. The force is applied through the die upper surface. A small-sliding contact pair is defined between the die and the spark plug hole and the boundary conditions at the supports are ensured by the kinematic coupling of nodes located on the surfaces where the supports are positioned (i.e. the zones highlighted in green in figure 3-b). A friction coefficient of 0.15 is used for the contact definition. The numerically applied force is equal to the experimentally determined level corresponding to 50% probability of failure of the cylinder heads. An elasto-plastic constitutive model with nonlinear isotropic hardening is used to simulate the material mechanical behaviour. 10 cycles are simulated; the stabilized response of the structure is obtained in the second cycle. With few exceptions, limited to elements surrounding the spark plug hole, the response of the whole structure is elastic.

In order to accurately assess the location of critical areas and the relative critical volume, an appropriate fatigue criterion has to be used. The probabilistic fatigue criterion, based on the framework proposed by Pessard et al [20] and modified by Le et al [9] to account for the specific fatigue behaviour of cast aluminium alloys, provides an attractive and efficient solution to reflect the competition between different fatigue damage mechanisms and describes the influence of defects on the HCF strength for a wide range of microstructural features, notably grain size, SDAS, pores size and multiaxial loading conditions. For our materials, two different fatigue criteria, the Dang Van criterion for crack initiation due to local plasticity and a Linear Elastic Fracture Mechanics (LEFM) criterion for crack initiation from micro-shrinkage pores are associated to describe the multiaxial high cycle fatigue strength. Note however that for the loading conditions used on both the specimens and the structure investigated in this communication, micro-shrinkage pores systematically control initiation of the principal fatigue crack and the fatigue strength. As such, it is proposed to simplify the approach used here, by only using a LEFM criterion, to assess the HCF response of the component. According to the LEFM, the range of the stress intensity factor (SIF) is expressed for surface defects [28] as:

$$\Delta K = 0.65 * \Delta\Sigma_I \sqrt{\pi \sqrt{area_{\max}}} \qquad (10)$$

with $\Delta\Sigma_I$ the maximum principal stress range and $area_{max}$ the critical defect size. The fatigue criticality (i.e. the Coefficient of Danger: *Cd*) is given dividing the stress intensity factor by its threshold $\Delta K_{th}^{R}$ :

$$Cd = \frac{\Delta K}{\Delta K_{th}^{R}} \qquad (11)$$

The influence of the load ratio, *R*, is captured by the stress intensity factor threshold using the correction introduced by Koutiri et al [8] :

$$\frac{\Delta K_{th}^{R}}{\Delta K_{th}^{R=0}} = \frac{1-R}{1-\kappa R} \qquad (12)$$

The modelling has two material parameters, κ and $\Delta K_{th}^{R=0}$. The parameter $area_{max}$ is derived from failure surface observations or extrapolation from the measured 2D pore size distribution. The two material parameters have been identified by Koutiri et al [8] using the experimental fatigue strength of alloy A with two load ratios: *R=-1* and *R=0.1*. Values of 0.59 and 2.29 $MPa\sqrt{m}$ are obtained for κ and $\Delta K_{th}^{R=0}$ respectively. The direct transfer of the LEFM

criterion identified on specimen to the component scale is based on two underlying assumptions: that the cracks retain an almost elliptical shape, which appears to be verified, as shown in Figure 6-d and that the stress intensity threshold and its variation with load ratio remains equivalent to that identified for the specimens.

This criteria has been implemented in the software used at PSA Groupe to perform fatigue analyses. As a first approach and according to the damage mechanisms observed on the specimens and the structure, the fatigue analysis is limited to the surface via the treatment of tensors provided by the membrane elements. Note that this approach implies that the stress gradient is neglected and can lead to an underestimation of the structure's strength. The authors are aware of the need to develop an appropriate strategy to account for the stress gradient. Work is currently underway to address this issue.

Figure 6-a and b show the simulation results. As a first approach, the analysis is performed by considering the average critical defect size observed on the specimens. The contour plot of the coefficient of danger is presented in Figure 6-a. Figure 6-b shows only the elements where the fatigue criterion value is greater than 90% of the maximum coefficient of danger. The predicted critical areas, located on the two branches of the water core agree well with the experimentally determined crack locations, shown in Figure 6-c.

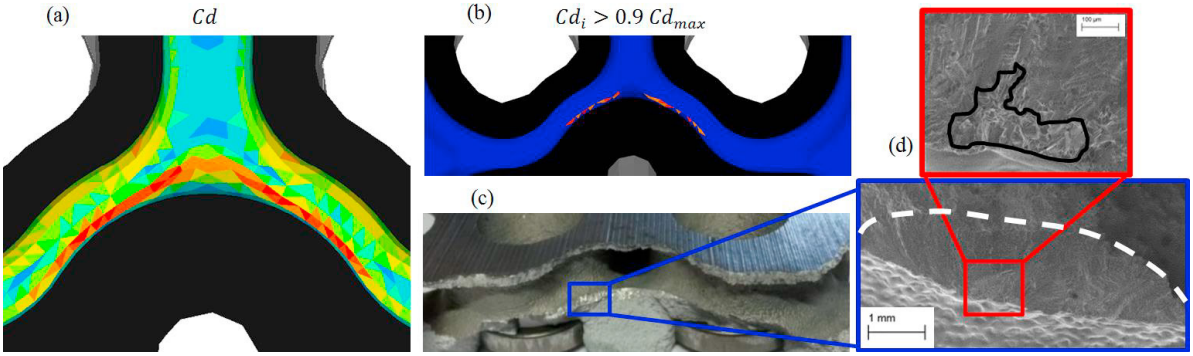


Figure 6 : (a) Contour plot of the coefficient of danger (Cd). (b)-(c) Comparison between the predicted and experimental locations of the fatigue critical areas in the cylinder heads. (b) Critical areas where the coefficient of danger is greater than 90% of the maximum value. (d) A typical fatigue failure surface observed on the cylinder head. Note that the crack shape is almost elliptical.

Because of the complex geometry in the critical areas, and the resulting complex stress fields, a significant variation in the coefficient of danger is observed around the most critical point, which has to be accounted for in the definition of the fatigue critical volume. It is proposed here to estimate the critical volume using the same methodology as that used for the specimens. That is by considering a subsurface volume with a 0.5 mm thickness. Various approaches have been proposed in the literature, to account for non-homogeneous stress fields in the prediction of fatigue life [23]. An extended comparison of these approaches for the investigated structure and materials, should be carried out, but as an initial approach, the method proposed by Sonsino et al [23] will be used here, where the critical area is identified as the region where the local damage variable is greater than 90% of the maximum value. These elements are highlighted in Figure 6-b. Assuming the continuity of the two major critical areas, the total critical volume is estimated to be 15 $mm^3$. It should be noted that this volume is significantly smaller (about ten times) than the critical loaded volume determined for the specimens. This is consistent with the large decreasing in the size of the average critical defect observed on the structure with respect to the specimens.

Table 4 summarizes the experimental and estimated average critical defect sizes for the cylinder heads. The average critical defect size is assessed using both the normalised procedure and the Makkonen approach and is compared to the observed average critical defect sizes. Again, the extrapolated values are in good agreement with the experimental critical defect size, for whichever methodology is used for the volume extrapolation.

| Alloy | Average critical defect size ($\sqrt{area_{max}}$) : Extrapolation from 2D measurements (µm) | | Average critical defect size ($\sqrt{area_{max}}$) : Observations on failure surface (µm) |
|---|---|---|---|
| | Normalised procedure [13] | Makkonen et al. [14] | |
| A | 164 | 185 | 162 |

Table 4 : Comparison between the experimental and the estimated average critical defect sizes for the structure, obtained with the normalized procedure and the Makkonen approach.

In summary, the systematic analysis of the failure surfaces and the defects at the origin of the principal fatigue cracks highlights a significant difference between the average critical defect size observed for the test specimens and the cylinder heads. Note that the fatigue criterion used here has been identified using the values for the specimens. This difference, which is close to 30%, results from a size effect, which is justified by the significant change of the loaded volume between the test specimens and the real structure. For the cases investigated here, the combination of the classical extreme value defect rating methodology with the available volume extrapolation methods and an accurate analysis of the loaded volume provides an efficient way to account for the size effect for the assessment of the average critical defect size at the origin of fatigue cracks.

## 4. Towards a fatigue design procedure for cylinder heads accounting for the size effect

The significant change of the average critical defect size between the test specimen and the real structure highlights a clear need to use a fatigue design methodology to account for the size effect. The satisfactory results obtained by extrapolating the average critical defect size leads to the possibility of proposing an appropriate design procedure, based on the combination of the extreme value defect rating methodology, volume extrapolation methods and the LEFM criterion presented earlier.

The design procedure is tested to predict the mean fatigue strength at $2x10^6$ cycles of the cylinder heads. The value of the load, obtained for the mean strength of the real structure, using the classical Dixon and Mood treatment of staircase results, is used for the numerical simulation. Three distinct fatigue analyses are performed. For the first two, the size effect is taken into account by considering the estimated average critical defect size on structure by using the normalised procedure and the Makonnen approach, respectively. For the last analysis, the size effect is neglected, and the average critical defect size observed for the specimens is used. The fatigue analysis results are presented in terms of contour plots of the coefficient of danger in Figure 7, a, b and c.

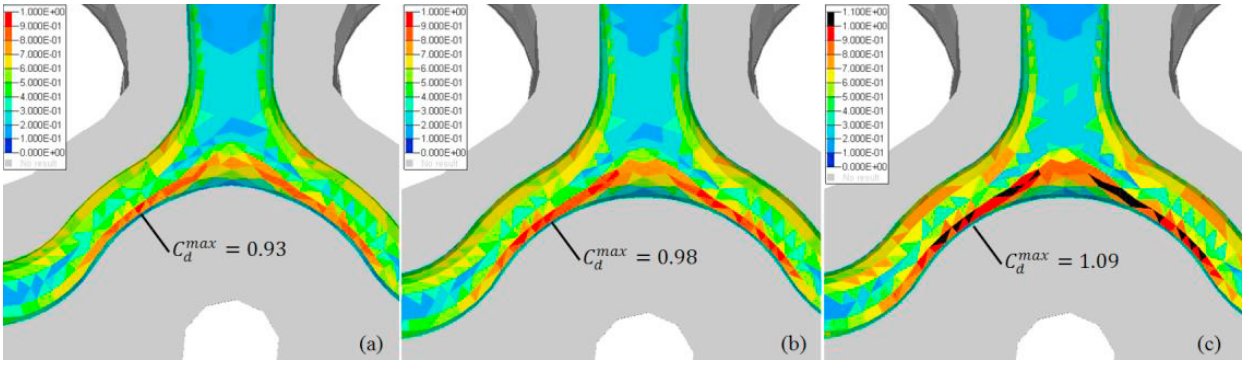


Figure 7 : Contour plots of the coefficient of danger obtained (a) using the estimated average critical defect size for the structure using the normalised procedure, (b) using the estimated average critical defect size for structure using the Makonnen approach and (c) by neglecting the volume effect.

Several remarks can be made regarding these results. First, an influence of the average critical defect size is logically observed on the values of the danger coefficient. A smaller average critical defect size results in the prediction of better strength for the structure. The location of the maximum danger coefficient, and more generally the spatial distribution of the danger coefficient is not affected by the chosen average critical defect size, which is logical. Secondly, neglecting the volume effect results in a conservative prediction of the component's strength, as shown in Figure 8-c. The maximum value of the danger coefficient, obtained considering the average critical defect size measured on the specimens is equal to 1.09, which corresponds to an overestimation of 9% of the strength of the structure. Conversely, accounting for the volume effect through the extrapolation of the average critical defect size for the structure results in a more accurate prediction of the strength. Indeed, even if this strength of the structure is slightly overestimated using the normalised procedure to account for size effect on average critical defect size, the analysis performed with the average critical defect size extrapolated using the Makkonen approach gives an accurate estimate of the strength of the cylinder heads. Finally, it is worth noting that neglecting the stress gradient does not seem to result in an important error for the prediction of the fatigue strength of the investigated structure. The assessment of the influence of the stress gradient on the fatigue strength prediction will be discussed in future communications.

## 5. Conclusion

Based on an accurate understanding of fatigue damage mechanism observed for both specimens and the structure, and a systematic analysis of fatigue failure surfaces, a clear link between the 2D micro-shrinkage pore size distributions and the mean fatigue strength has been established. This has been achieved by combining the extreme value defect rating methodology introduced by Murakami [12] with volume extrapolation methods. Two volume extrapolation methods were tested: a ASTM standardised procedure and the approach proposed by Makkonen et al [14], each one of them gives satisfactory results in terms of the average critical defect size for the investigated materials and volume changes.

This exercise, combined with an accurate analysis of the critically loaded volume for the specimens and the structure, highlights a significant volume effect between the test specimens, used to identify the fatigue criterion, and the structure. This volume effect is identified through the average critical defect size, which decreased by approximately 30% between the specimens and the structure as a result of a change in the critically loaded volume.

The good results obtained for the average critical defect size assessment provide the opportunity to propose a relevant fatigue design procedure to account for the size effect, based on the combination of the extreme value defect rating methodology, volume extrapolation methods and a classical LEFM criterion. This approach is used to predict the fatigue strength of the cylinder heads and to assure a better quality fatigue strength prediction compared to an equivalent approach neglecting the volume effect.

## Acknowledgement

This work was financially supported by PSA Groupe and the French National Agency for Research and Technology.

## References

[1] ASTM E155-15, Standard Reference Radiographs for Inspection of Aluminum and Magnesium Castings, ASTM International, West Conshohocken, PA, 2015, www.astm.org

[2] Le, V. D., Morel, F., Bellett, D., Saintier, N., & Osmond, P. (2016). Multiaxial high cycle fatigue damage mechanisms associated with the different microstructural heterogeneities of cast aluminium alloys. Materials Science and Engineering: A, 649, 426-440.

[3] Imade Koutiri, Daniel Bellett, Franck Morel, Louis Augustins, and Jérome Adrien. High cycle fatigue damage mechanisms in cast aluminium subject to complex loads. International Journal of Fatigue, 47(0):44 – 57, 2013.

[4] Q.G. Wang, D Apelian, and D.A Lados. Fatigue behavior of a356-t6 aluminum cast alloys. part i. effect of casting defects. Journal of Light Metals, 1(1):73 – 84, 2001.

[5] D.L McDowell, K Gall, M.F Horstemeyer, and J Fan. Microstructure-based fatigue modeling of cast a356-t6 alloy. Engineering Fracture Mechanics, 70(1):49 – 80, 2003.
[6] J-Y. Buffière, S. Savelli, P.H. Jouneau, E. Maire, and R. Fougères. Experimental study of porosity and its relation to fatigue mechanisms of model alsi7mg0.3 cast al alloys. Materials Science and Engineering: A, 316(12):115– 126, 2001.
[7] Houria, M. I., Nadot, Y., Fathallah, R., Roy, M., & Maijer, D. M. (2015). Influence of casting defect and SDAS on the multiaxial fatigue behaviour of A356-T6 alloy including mean stress effect. International Journal of Fatigue, 80, 90-102.
[8] Koutiri, I., Bellett, D., Morel, F., & Pessard, E. (2013). A probabilistic model for the high cycle fatigue behaviour of cast aluminium alloys subject to complex loads. International Journal of Fatigue, 47, 137-147.
[9] Le, V. D., Morel, F., Bellett, D., Saintier, N., & Osmond, P. (2016). Simulation of the Kitagawa-Takahashi diagram using a probabilistic approach for cast Al-Si alloys under different multiaxial loads. International Journal of Fatigue, 93, 109-121.
[10] Rotella, A., Nadot, Y., Augustin, R., Piellard, M., & L'Heritier, S. (2017). Defect size map for cast A357-T6 component under multiaxial fatigue loading using the Defect Stress Gradient (DSG) criterion. Engineering Fracture Mechanics, 174, 227-242.
[11] Le, V. D. (2016). Etude de l'influence des hétérogénéités microstructurales sur la tenue en fatigue à grand nombre de cycles des alliages d'aluminium de fonderie (Doctoral dissertation, Paris, ENSAM).
[12] Murakami, Y. (2002). Metal fatigue: effects of small defects and nonmetallic inclusions. Elsevier.
[13] ASTM E2283-03, Standard Practice for Extreme Value Analysis of Nonmetallic Inclusions in Steel and Other Microstructural Features, ASTM International, West Conshohocken, PA, 2003, www.astm.org
[14] Makkonen, L., Rabb, R., & Tikanmäki, M. (2014). Size effect in fatigue based on the extreme value distribution of defects. Materials Science and Engineering: A, 594, 68-71.
[15] Le, V. D., Saintier, N., Morel, F., Bellett, D., & Osmond, P. (2018). Investigation of the effect of porosity on the high cycle fatigue behaviour of cast Al-Si alloy by X-ray micro-tomography. International Journal of Fatigue, 106, 24-37.
[16] Mu, P., Nadot, Y., Nadot-Martin, C., Chabod, A., Serrano-Munoz, I., & Verdu, C. (2014). Influence of casting defects on the fatigue behavior of cast aluminum AS7G06-T6. International Journal of Fatigue, 63, 97-109.
[17] Koutiri, I., Bellett, D., Morel, F., Augustins, L., & Adrien, J. (2013). High cycle fatigue damage mechanisms in cast aluminium subject to complex loads. International Journal of Fatigue, 47, 44-57.
[18] Koutiri, I. (2011). Effet des fortes contraintes hydrostatiques sur la tenue en fatigue des matériaux métalliques (Doctoral dissertation, Arts et Métiers ParisTech).
[19] Serrano-Munoz, I., Buffiere, J. Y., Verdu, C., Gaillard, Y., Mu, P., & Nadot, Y. (2016). Influence of surface and internal casting defects on the fatigue behaviour of A357-T6 cast aluminium alloy. International Journal of Fatigue, 82, 361-370.
[20] Pessard, E., Bellett, D., Morel, F., & Koutiri, I. (2013). A mechanistic approach to the Kitagawa–Takahashi diagram using a multiaxial probabilistic framework. *Engineering Fracture Mechanics*, *109*, 89-104.
[21] Koutiri, I., Bellett, D., Morel, F., & Pessard, E. (2013). A probabilistic model for the high cycle fatigue behaviour of cast aluminium alloys subject to complex loads. *International Journal of Fatigue*, *47*, 137-147.
[22] Flavenot, J. F., & Skalli, N. (1989). A critical depth criterion for the evaluation of long-life fatigue strength under multiaxial loading and a stress gradient. In *ECF5, Lisbon 1984*.
[23] Sonsino, C. M., Kaufmann, H., & Grubišić, V. (1997). *Transferability of material data for the example of a randomly loaded forged truck stub axle* (No. 970708). SAE Technical Paper.
[24] Bellett, D., Taylor, D., Marco, S., Mazzeo, E., Guillois, J., & Pircher, T. (2005). The fatigue behaviour of three-dimensional stress concentrations. *International journal of Fatigue*, *27*(3), 207-221.
[25] Morel, F., & Palin-Luc, T. (2002). A non-local theory applied to high cycle multiaxial fatigue. *Fatigue & Fracture of Engineering Materials & Structures*, *25*(7), 649-665.
[26] Papadopoulos, I. V., & Panoskaltsis, V. P. (1996). Invariant formulation of a gradient dependent multiaxial high-cycle fatigue criterion. *Engineering Fracture Mechanics*, *55*(4), 513-528.
[27] Nadot, Y., & Billaudeau, T. (2006). Multiaxial fatigue limit criterion for defective materials. *Engineering fracture mechanics*, *73*(1), 112-133.
[28] Murakami, Y. (1986). Stress intensity factors handbook. *Soc. Mater. Sci., Japan*.